Application of second harmonic imaging microscopy to assess structural changes in optic nerve head structure *ex vivo*

Donald J. Brown
University of California, Irvine
School of Medicine
The Eye Institute
Orange, California 92868

Naoyuki Morishige
Yamaguchi University
Graduate School of Medicine
Department of Ophthalmology
Yamaguchi, Japan

Aneesh Neekhra
Don S. Minckler
James V. Jester
University of California, Irvine
School of Medicine
The Eye Institute
Orange, California 92868

Abstract. Glaucoma represents the second leading cause of blindness worldwide. While both age and intraocular pressure (IOP) are well-recognized risk factors for this disease, the underlying pathologic process involves the accelerated death of retinal ganglion cells (RGCs) that is associated with progressive loss of vision. The loss of RGCs has been postulated to occur primarily by injury to axons in the optic nerve head (ONH) due to its anatomic features and the mechanical vulnerability of the lamina cribrosa, the specialized ONH zone comprised of collagen beams that define the channels or pores through which axon bundles exit the eye. Recent advances in multiphoton microscopy using femtosecond lasers that generate second harmonic (SH) signals from collagen allows for direct optical imaging of the lamina cribrosa. We assess the application of SH generated microscopy (SHG) to the study of the ONH, and test the general hypothesis that increasing intraocular pressure in the same eye results in the movement of ONH collagen beams leading to distortion of the lamina cribrosa channels and compression of the axon bundles. [DOI: 10.1117/1.2717540]

Keywords: second harmonic imaging microscopy; optic nerve head; lamina cribrosa; glaucoma.

Paper 06302LR received Oct. 26, 2006; revised manuscript received Jan. 31, 2007; accepted for publication Jan. 31, 2007; published online Apr. 13, 2007.

1 Introduction

Elevation of intraocular pressure may lead to progressive optic atrophy defined as a loss of retinal ganglion cells (RGCs) accompanied by visual field defects. Compression of axonal bundles by stretching and fibrosis of the intervening connective tissue in the lamina cribrosa associated with increasing age and intraocular pressure levels have been shown to be important to the pathophysiology of glaucomatous damage.[1] Mechanical effects of elevated eye pressure include blockage of both orthograde and especially retrograde axonal transport as axons traverse the lamina cribrosa.[2] A growing body of evidence suggests that impedance of axonal transport accelerates apoptosis of RGCs. While the loss of RGCs likely represents the critical aspect of the disease process,[3] the physical and mechanical properties of the lamina cribrosa undoubtedly play a central role in the pathogenesis of glaucoma. Overall, it is generally hypothesized that increasing intraocular pressure (IOP) results in movement of the ONH collagen beams, eventually leading to distortion of the lamina cribrosa pores and the exiting axon bundles.

While numerous studies have examined the lamina cribrosa, a number of technical problems with traditional methodologies have limited our ability to analyze the details of structural change induced by increased eye pressure. Most investigations by necessity have utilized fixed postmortem tissues, serial sectioning, and staining procedures for microscopic evaluation. These methods have been valuable but limited by artifacts common to tissue processing. Additionally, standard histology methods are labor intensive and expensive. Here, we demonstrate an alternate technique using optical imaging of second harmonic generated (SHG) signals from collagen within the lamina cribrosa.

The technique relies on the observation made by Freund, Deutsch, and Sprecher, who demonstrated that laser light generates SH signals from biologic tissues.[4] SH signals are generated when two near-infrared photons interact with a highly polarized and noncentro-symmetric material such as collagen. This interaction generates a single, visible photon having twice the energy and half the wavelength.[5] With the recent advances in multiphoton microscopy using femtosecond lasers with high energy and short pulses focused within very small volumes of tissue, the application of SHG has been greatly expanded and includes studies of collagen and tubulin organization.[6]

2 Visualization of the Optic Nerve Head and Surrounding Tissue

To examine whether similar collagen-based signals could be obtained from the human optic nerve head (ONH), two human

Address all correspondence to Donald Brown, Ophthalmology, University of California, Irvine, 101 The City Drive, Building 55 Room 208, Orange, CA 92868; Tel: 714-456-7368; Fax: 714–456–5073; E-mail: dbrown@uci.edu

1083-3668/2007/12(2)/024029/5/$25.00 © 2007 SPIE

autopsy eyes not suitable for transplantation and with no identifiable private information (not considered human subjects research under exemption number 4) were obtained from a local eye bank. These eyes were oriented and marked to reflect orientation (superior and inferior), and dissected to remove the anterior cap and vitreous, exposing a view of the ONH under a surgical microscope. Using a 6-mm trephine, a block of tissue containing the ONH was removed from the posterior pole. This disk of tissue was fixed with 4% paraformaldehyde in buffered saline at 4°C overnight, then placed on a coverslip and imaged.

Specimens were placed on an Axiovert 200 microscope configured specifically for multiphoton applications (Zeiss, Jena, Germany), and imaged using a Plan ApoChromat 20× objective (NA=0.75, Zeiss). Two-photon SH signals are generated using a mode-locked titanium:sapphire laser (Chameleon®, Coherent Incorporated, Santa Clara, California) producing a 150-fs pulse with a repetition rate of 90 MHz and set to deliver 48-mW average power at the focal plane of the objective. Backward-scattered SHG signals were detected using the Meta detector on the Zeiss 510, set to detect emission frequencies from 380 to 420 nm after passing an HFT KP650 beamsplitter and a BG 39 infrared filter to remove the excitation signal. The pinhole was set to the maximal open setting for this application, and the samples were scanned using a 5-μm z-axis step size to generate 3-D data to a depth of 300 μm within the ONH. All images were recorded as 8-bit, 512×512 images. 3-D datasets were reconstructed using the LSM Image Examiner (Carl Zeiss, Germany).

As shown in Fig. 1, the SH signals obtained from the posterior aspect of the ONH are remarkably similar to images obtained by scanning electron microscopy [compare Fig. 1(a), SEM, to Fig. 1(b), SHG]. Further, the datasets obtained by imaging from the anterior to posterior aspect [through the retina and optic nerve head in Fig. 1(c)] demonstrate that the second harmonic signals are easily detected to a depth of 300 μm. These data suggest that the collagenous component of the lamina cribrosa can generate significant second harmonic signals that are easily interpretable and obtained at a frame rate of 3.93 s (1.6 μs per pixel).

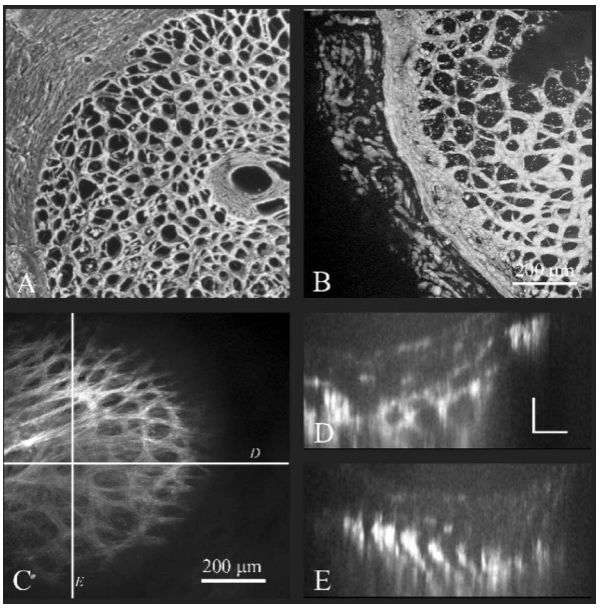

Fig. 1 Second harmonic images of the lamina cribrosa. 3-D datasets of the lamina were collected using SH signals from the collagen fibrils. (a) shows an archived image of scanning electron microscopy of the posterior aspect of the LC in comparison to an equivalent plane using SHG with a 20× objective (b). (c) represents a maximum intensity projection SHG dataset comprised of 60 optical images (20×objective) separated by 5-μm steps through the anterior ONH. (d) and (e) represent *xz* and *yz* projections, respectively, of the dataset along the axis lines *D* and *E* indicated in (c). The white scale bar in (d) represents 100 μm in *z* and *x* planes [same scale in (e)].

3 Reconstruction of the Optically Sectioned Lamina Cribrosa

We then proceeded to image the ONH from the posterior aspect of two eyes, collecting 3-D datasets to a depth of 200 μm and encompassing the entire scleral canal region using a 10× Plan NeoFluar objective (NA=0.3). Figure 2 demonstrates a montage of 12 maximum intensity projections from two autopsy eyes; one eye [Fig. 2(a)], where the optic nerve was cut obliquely to reveal deeper layers of the lamina cribrosa, and the other eye [Fig. 2(b)], cut parallel to the scleral surface to reveal the posterior region of the lamina cribrosa. In Fig. 2(a), the thick black line indicates where the optic nerve was trimmed at an angle deeper into the lamina cribrosa. Interestingly, the oblique section of the optic nerve head region shows that the more anterior collagen [right side of Fig. 2(a)] is distinct and arranged in a more radial pattern than in the more posterior region [left side of Fig. 2(a)]. This difference can also be noted in Fig. 1 [compare Figs. 1(c) and 1(b)]. The montage image from Fig. 2(b) was used to determine the pore size distribution by region using MetaMorph (Molecular Devices Corporation, Downingtown, Pennsylvania). Essentially, the scleral canal was divided into inferior, superior, nasal, and temporal quadrants and the area of the pores measured by two independent observers using the region measurement subroutine. The reproducibility of these measurements was checked by assessing the percent error and Pearson correlation between the two measurements in the

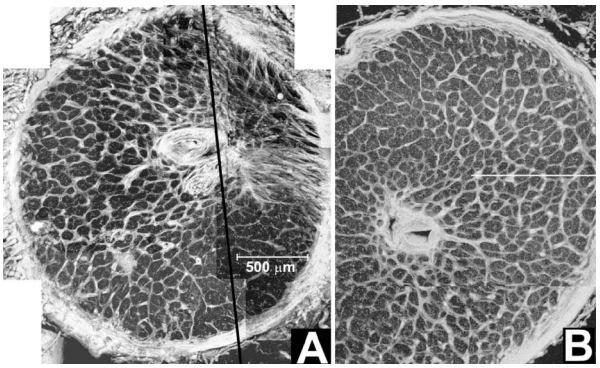

Fig. 2 Second harmonic images of the posterior lamina cribrosa. As described in the text, 3-D datasets of the lamina were collected using SH signals from the collagen fibrils using a 10× objective. (a) shows a composite of maximum intensity projection SHG datasets taken from a 59-yr-old eye, while (b) shows a similar composite of a 63-yr-old eye. Note the black line in (a) explained in the text.

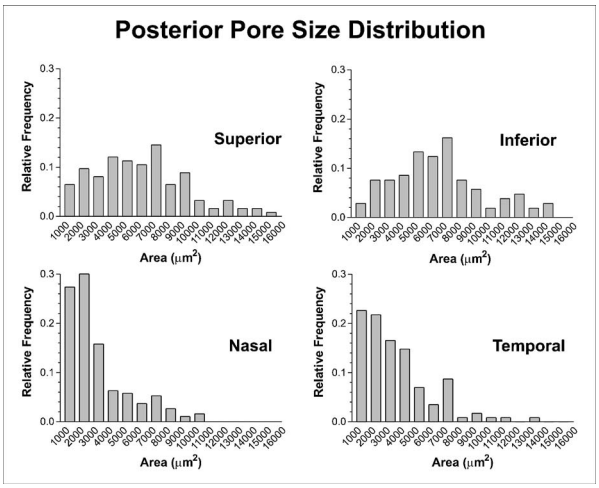

Fig. 3 Posterior pore size and geographic location. The image shown in Fig. 2(b) was divided into four regions using the central artery as a center. Using MetaMorph software, the pores were individually demarcated and areas recorded for each pore. A frequency histogram was constructed to demonstrate the size and frequency of the pore size in each region.

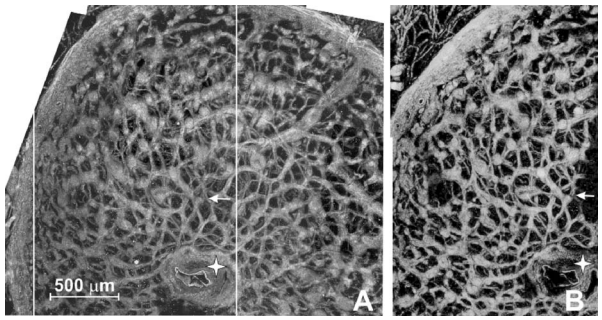

Fig. 4 Second harmonic images of the posterior lamina cribrosa. As described in the text, 3-D datasets of the lamina were collected using SH signals from the collagen fibrils. (a) shows a montage composite of the maximum intensity projections of SHG datasets taken from a fresh unfixed 85-yr-old eye (10× objective). After those data were taken, the pressure was raised to approximately 50-mm Hg and new datasets were obtained. The white box in (a) shows the equivalent region assessed before (0-mm Hg) and after raising the pressure [50-mm Hg, (b)]. Note both the central artery and vein (white stars) appear more patent in the pressurized eye, suggesting the affects of increased pressure in the globe. The white arrows are placed to demonstrate similar positions in the two images.

same region of the lamina cribrosa (LC).[7] This analysis indicated each observer-measured area with an average difference of 6 to 9% of the value measured, and Pearson *r* values of correlation of 0.99 and 0.98 for the two selected images.

Figure 3 and Table 1 show the frequency distribution of pores by geographic region. Here, the data suggests regional differences in pore size. There is a tendency for smaller pores to be more frequent in the temporal and nasal quadrants, while the inferior and superior quadrants have a broader and larger size distribution, which is entirely consistent with the literature.[8] By analysis of variance (ANOVA), there was a significant difference ($p < 0.001$) between pores size and optic nerve head region. However, given the large variation in pore sizes in each, and noting that these data represent a single eye under no pressure, no strong conclusion can be drawn.

4 Reconstruction of the Optically Sectioned Lamina Cribrosa with an Increase in Ocular Pressure

The experiments described before demonstrate that: 1. the lamina cribrosa can be imaged in fixed tissues, and 2. the structure can be optically sectioned from both the anterior and posterior face of the globe. It should then be possible to image this structure in the whole, intact eye without fixation. This would minimize artifacts attributed to either dissection or fixation of the globe. Additionally, one should be able to pressurize the intact eye and acquire datasets at various controlled levels of pressure in the same eye. To demonstrate this, we obtained a single fresh eye, 85 years, 12 hours postmortem. The eye was cannulated with a 25-gauge suture less trocar and cannula system attached to a reservoir of buffered saline solution. Care was taken to maintain the eye at the same level as the reservoir. The protruding optic nerve was removed at the level of the sclera using a disposable cryostat blade. The entire eye was placed onto the microscope and held in place with moistened cotton gauze so that the posterior aspect of the ONH was oriented above the objective. The reservoir was raised to the level of the stage, and images across the entire scleral canal and to a depth of 300 μm were collected (baseline pressure). After collecting these data, the reservoir was raised to a height of 27 in. (~50-mm Hg). This represents an elevated pressure that has been associated with both primary and chronic angle-closure glaucoma.[9,10] The sample was maintained at this pressure for 30 min and the entire area imaged again. As demonstrated in Fig. 4, comparison of the reconstructed images from two distinct pressures show little difference except for a more patent central artery and vein (star). Interestingly, the overall intensity of the now pressurized eye [Fig. 4(b)] was higher, which may be explained by compression of the collagen fibrils, so that more fibrils are present in less volume (as indicated by the *xz* and *yz* projections, data not shown). Also possible is that structural changes in the collagen with pressure may result in more efficient reflection of the SHG signal, as suggested by the work of Tan et al.,[11] who demonstrated that structural changes in corneal collagen increased the SHG signal. However, as these data represent a single eye, no conclusion for this observation can be obtained and requires more experimentation. Nonetheless,

Table 1 Posterior pore size by geographical region. The Kruskal-Wallis test for non-Gaussian distributions suggests significant differences ($p < 0.001$) between the superior and inferior regions and the nasal or temporal region. No difference was noted between the superior and inferior or nasal and temporal regions.

Region	Mean (μm^2)	Standard deviation
Superior	4938	3201
Inferior	5900	4129
Nasal	1969	2118
Temporal	2485	4129

thinning and compression of the lamina has been demonstrated previously to occur in the primate eye with increasing pressure.[1,12,13] Of note, this eye was from an older individual (85 years) and in comparison to the younger eyes (Figs. 1 and 2) that we have examined, the collagen beams appear much thicker with a corresponding reduction in pore size, which is consistent with the literature, indicating a thickening of collagen and reduction in pore size with aging (reviewed in Ref. 1).

When the datasets shown in Figs. 4(a) and 4(b) were analyzed for pore size, distinct differences were noted. The pores were measured manually using MetaMorph software, and the differences between the same pore at the two different pressures were analyzed by a paired *t*-test. The data suggested that the mean pore size was slightly but significantly enlarged in the pressurized eye ($p < 0.001$, paired *t*-test, Table 2). Most interesting is the paired, rank-ordered scatter plot (Fig. 5) that shows the change, or lack of change, of individual pores (each point is a single pore). In this analysis, pores were assigned to four groups: central, mid-central, mid-peripheral, and peripheral pores [depicted by the arcs in Fig. 5(a)]. Each pore was marked and measured for area using the MetaMorph software package. As shown in the rank-ordered scatter plot [Fig. 5(b)], individual pores generally increased in size with pressure (points to the left of the identity line increased in area). However, many pores were also reduced in size (points to the right of the identity line). When pores were plotted based on their location assignment, an exciting result was noted. That is, the pores in the periphery of the ONH generally decreased in size (filled diamonds). Pores near the central vessels of the ONH were relatively unaffected by the increase in pressure. Additionally, linear regression analysis suggested that smaller pores are more responsive (relative change in size) than larger pores and more likely to be reduced in size. Also of note, the average percent change in area in this dataset was 30% (with a large standard deviation of 26%), indicating that the average change in area that accompanied the change in pressure was several times larger than the 6 to 9% difference in measurement noted between observers (as described with Fig. 2).

Table 2 Change in posterior pore size with increased intraocular pressure. The images shown in Fig. 4 were analyzed for pore size area after assignment of the regions shown in Fig. 5.

Region	0-mm Hg mean (μm^2)	50-mm Hg mean (μm^2)
Central	2106±1338[a]	2226±1516
Mid-central	1805±956	2048±1069
Mid-peripheral	1894±1404	2094±165
Peripheral	2428±1612	2197±1453

[a]Standard deviation.

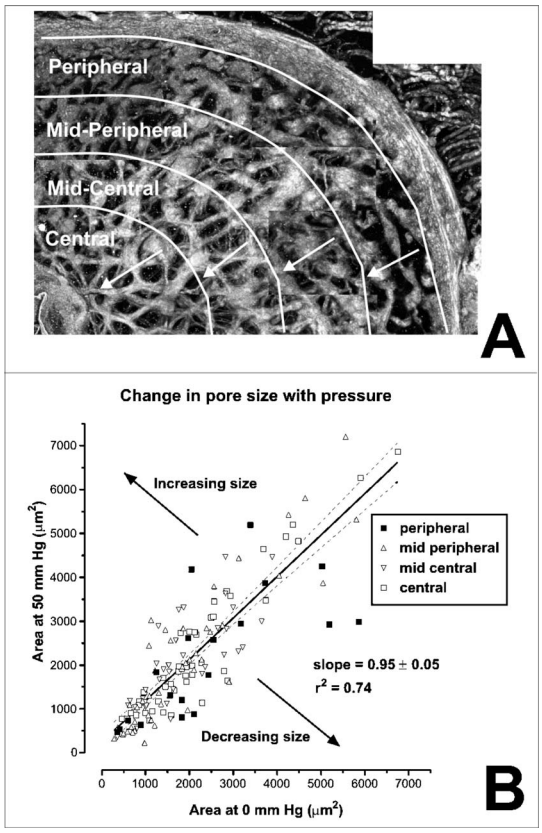

Fig. 5 Regional analysis of pore size changes with increased ocular pressure. (a) shows the superior temporal quadrant of the eye described in Fig. 4. The pores were measured based on their position defined by the white arcs and compared to their corresponding size at 50-mm Hg pressure. (b) shows the results of this analysis, where each pore is plotted against itself at higher pressure (each point is a single pore). Central region pores are in open squares, while pores in the peripheral region are in filled squares. The arrows indicate the displacement expected with an increase or decrease in pore size after elevating the pressure. The black line indicates the linear regression of the data with its 95% confidence interval (dashed lines).

To our knowledge, these data are unique in that a change in ocular pressure increases the size of pores in the mid-central and mid-peripheral regions of the ONH, while pores at the periphery generally collapse. This finding generally correlates with the anatomic and well-known clinical topography of optic nerve injury in glaucoma, in which the peripherally located ganglion cells responsible for peripheral visual field, projecting to the peripheral optic nerve, are most vulnerable early in the injury process.[14]

These data support the general hypothesis that increasing intraocular pressure results in the movement of the ONH collagen beams, which distorts of the lamina cribrosa pores and compresses axon bundles. These data also have implications for understanding the effect of IOP on the mechanical properties of the ONH and the susceptibility of axons to these changes. It has long been appreciated that optic disk deformation and cupping noted clinically in glaucoma reflect the stretching and compression of the extracellular matrix of the lamina cribrosa, and our data are certainly consistent with this and suggest that the cupping involves preservation of central architecture and a corresponding compression near the periphery of the ONH. Further, as glaucoma is associated with geographically demarcated visual field loss, whose axons pass through pores in the periphery of the ONH (demonstrated in mapping studies[14,15]), our data suggest a correlation between pressure, pore size, and structural displacement in the peripheral laminar region more susceptible to ganglion cell loss.

While this work illustrates the usefulness of SHG in the examination of the ONH, SHG has been applied to other ocular tissues. Notably, the cornea, with the very precise ordering of collagen fibrils, has been studied in a variety of species and pathologic conditions.[11,16–18] In addition, other investigators have been applying this technology to the study of *ex-vivo* tissues deeper within the eye, including the lens.[19] and the retinal pigmented epithelium.[20] We expect that the application of SHG to studies of the ONH will lead to important new information concerning the 3-D structure of the lamina cribrosa. Already, the data indicate that the collagenous structure of the lamina cribrosa is composed of at least two distinct arrangements of fibrils with the collagen layer immediately below the retina at its anterior face marked by longer, more linear fibrils arrayed in a more radial fashion [Fig. 1(c)]. The collagen fibrils at the posterior face of the lamina are composed of more highly branched fibrils that form a complex, interwoven network [Fig. 1(b)]. These data, though preliminary, suggest that fibrils are affected by pressure differently with their geographic region (Fig. 5). This finding can be of significant value when analyzing pathological changes in ocular ischemic diseases, as a recent study has suggested a throttle mechanism in the central retinal vein in the region of the lamina cribrosa.[21] Further, SHG can be rapidly applied to the assessment of a variety of common animal models of glaucoma and utilized to identify the effects of age, ethnicity, and disease-related changes in human tissue. The data generated can be of great clinical significance and can be a valuable addition to glaucoma screening tools. Finally, the data generated by these studies can be applied to the development of a biomechanical finite element model[22] of the ONH.

Acknowledgments

The authors thank Glaucoma Research Foundation (D.J.B.), Japan Eye Bank Association (N.M.), The Glaucoma Foundation (D.S.M.), NIH grants EY07348 and EY016663 (J.V.J.), and support grants from Research to Prevent Blindness, Incorporated, The Skirball Program in Molecular Ophthalmology, and The Discovery Eye Foundation.

References

1. C. F. Burgoyne, J. C. Downs, A. J. Bellezza, J. K. Suh, and R. T. Hart, "The optic nerve head as a biomechanical structure: a new paradigm for understanding the role of IOP-related stress and strain in the pathophysiology of glaucomatous optic nerve head damage," *Prog. Retin Eye Res.* **24**, 39–73 (2005).
2. D. S. Minckler and G. L. Spaeth, "Optic nerve damage in glaucoma," *Surv. Ophthalmol.* **26**, 128–148 (1981).
3. M. E. Pease, S. J. McKinnon, H. A. Quigley, L. A. Kerrigan-Baumrind, and D. J. Zack, "Obstructed axonal transport of BDNF and its receptor TrkB in experimental glaucoma," *Invest. Ophthalmol. Visual Sci.* **41**, 764–774 (2000).
4. I. Freund, M. Deutsch, and A. Sprecher, "Connective tissue polarity. Optical second-harmonic microscopy, crossed-beam summation, and small-angle scattering in rat-tail tendon," *Biophys. J.* **50**, 693–712 (1986).
5. W. Mohler, A. C. Millard, and P. J. Campagnola, "Second harmonic generation imaging of endogenous structural proteins," *Methods* **29**, 97–109 (2003).
6. P. J. Campagnola and L. M. Loew, "Second-harmonic imaging microscopy for visualizing biomolecular arrays in cells, tissues and organisms," *Nat. Biotechnol.* **21**, 1356–1360 (2003).
7. H. F. Li, W. M. Petroll, T. Moller-Pedersen, J. K. Maurer, H. D. Cavanagh, and J. V. Jester, "Epithelial and corneal thickness measurements by in vivo confocal microscopy through focusing (CMTF)," *Curr. Eye Res.* **16**, 214–221 (1997).
8. J. B. Jonas, C. Y. Mardin, U. Schlotzer-Schrehardt, and G. O. Naumann, "Morphometry of the human lamina cribrosa surface," *Invest. Ophthalmol. Visual Sci.* **32**, 401–405 (1991).
9. D. M. Robertson, L. Li, S. Fisher, V. P. Pearce, J. W. Shay, W. E. Wright, H. D. Cavanagh, and J. V. Jester, "Characterization of growth and differentiation in a telomerase-immortalized human corneal epithelial cell line," *Invest. Ophthalmol. Visual Sci.* **46**, 470–478 (2005).
10. Z. Alsagoff, T. Aung, L. P. Ang, and P. T. Chew, "Long-term clinical course of primary angle-closure glaucoma in an Asian population," *Ophthalmology* **107**, 2300–2304 (2000).
11. H. Y. Tan, S. W. Teng, W. Lo, W. C. Lin, S. J. Lin, S. H. Jee, and C. Y. Dong, "Characterizing the thermally induced structural changes to intact porcine eye, part 1: second harmonic generation imaging of cornea stroma," *J. Biomed. Opt.* **10**, 054019 (2005).
12. A. J. Bellezza, C. J. Rintalan, H. W. Thompson, J. C. Downs, R. T. Hart, and C. F. Burgoyne, "Anterior scleral canal geometry in pressurised (IOP 10) and non-pressurised (IOP 0) normal monkey eyes," *Br. J. Ophthamol.* **87**, 1284–1290 (2003).
13. C. F. Burgoyne, J. C. Downs, A. J. Bellezza, and R. T. Hart, "Three-dimensional reconstruction of normal and early glaucoma monkey optic nerve head connective tissues," *Invest. Ophthalmol. Visual Sci.* **45**, 4388–4399 (2004).
14. D. S. Minckler, "The organization of nerve fiber bundles in the primate optic nerve head," *Arch. Ophthalmol. (Chicago)* **98**, 1630–1636 (1980).
15. D. S. Minckler, A. H. Bunt, and I. B. Klock, "Radioautographic and cytochemical ultrastructural studies of axoplasmic transport in the monkey optic nerve head," *Invest. Ophthalmol. Visual Sci.* **17**, 33–50 (1978).
16. W. Lo, S. W. Teng, H. Y. Tan, K. H. Kim, H. C. Chen, H. S. Lee, Y. F. Chen, P. T. So, and C. Y. Dong, "Intact corneal stroma visualization of GFP mouse revealed by multiphoton imaging," *Microsc. Res. Tech.* **69**, 973–975 (2006).
17. S. W. Teng, H. Y. Tan, J. L. Peng, H. H. Lin, K. H. Kim, W. Lo, Y. Sun, W. C. Lin, S. J. Lin, S. H. Jee, P. T. C. So, and C. Y. Dong, "Multiphoton autofluorescence and second-harmonic generation imaging of the *ex vivo* porcine eye," *Invest. Ophthalmol. Visual Sci.* **47**, 1216–1224 (2006).
18. N. Morishige, W. M. Petroll, T. Nishida, M. C. Kenney, and J. V. Jester, "Noninvasive corneal stromal collagen imaging using two-photon-generated second-harmonic signals," *J. Cataract Refractive Surg.* **32**, 1784–1791 (2006).
19. W. Pendergrass, P. Penn, D. Possin, and N. Wolf, "Accumulation of DNA, nuclear and mitochondrial debris, and ROS at sites of age-related cortical cataract in mice," *Invest. Ophthalmol. Visual Sci.* **46**, 4661–4670 (2005).
20. A. Bindewald-Wittich, M. Han, S. Schmitz-Valckenberg, S. R. Snyder, G. Giese, J. F. Bille, and F. G. Holz, "Two-photon-excited fluorescence imaging of human RPE cells with a femtosecond Ti:Sapphire laser," *Invest. Ophthalmol. Visual Sci.* **47**, 4553–4557 (2006).
21. T. H. Williamson, "A 'throttle' mechanism in the central retinal vein in the region of the lamina cribrosa," *Br. J. Ophthamol.* (2006).
22. A. J. Bellezza, R. T. Hart, and C. F. Burgoyne, "The optic nerve head as a biomechanical structure: initial finite element modeling," *Invest. Ophthalmol. Visual Sci.* **41**, 2991–3000 (2000).